RSC Advances

ROYAL SOCIETY OF CHEMISTRY

www.rsc.org/advances

Effect of microstructure and Sn/C ratio in SnO_2/Graphene nanocomposites for lithium-ion battery performance.

Mahbuba Ara, Kapila Wadumesthrige, Tiejun Meng, Steven O. Salley and K. Y. Simon Ng*

Department of Chemical Engineering and Materials Science, Wayne State University, Detroit, MI 48202

* Corresponding author. Tel.: +1 313 577 3805; fax: +1 313 577 8171.

E-mail address: sng@wayne.edu (K. Y. Simon Ng).

Abstract

Sn based nanocomposite anodes with pristine graphene matrix were synthesized in order to investigate the performance improvements that related to the microstructure variation. Four nanocomposites with varying SnO_2 contents (25, 43, 60, and 82 wt%) were prepared with a controlled hydrothermal synthesis route. TEM measurements indicated that 25/75 wt% SnO_2/graphene nanocomposite had the highest dispersivity with 2-3 nm particle size and ~2 nm inter-particle spacing. Increasing SnO_2 content led to increase of the particle size and decrease of inter-particle spacing. For the anode with more dispersed and smaller nanoparticles, the capacity retention and rate capability was noticeably improved compared with anodes that have clusters of SnO_2 nanopartices. 25/75 wt% SnO_2/graphene nanocomposite exhibited enhanced specific capacity of 662 mAh/g after 150 cycles when discharged/charged at 50 mA/g. It also demonstrated an outstanding rate capability of 525, 445 and 230 mAh/g at higher current densities of 300, 500 and 1000 mA/g, respectively. TEM and EIS study revealed that after 100 electrochemical cycles, the nanoparticles retained the original size of 2-3 nm and cell's charge transfer resistance decreased by 52%.

Keywords: Tin oxide; nanocomposite anode; lithium-ion batteries; particle spacing.

1. Introduction

While rechargeable lithium-ion batteries are the predominant power sources for portable electronic devices, more advanced lithium-ion batteries with high energy and power density, rate capability and excellent cycling stability are required to achieve economically-competitive electric vehicles. Commercial lithium-ion batteries are usually based on carbonaceous anode materials, like graphite, which do not exhibit the problem of dendrite formation experienced in the initially employed lithium metal anode.[1,2] . However, graphite displays a low theoretical charge capacity (372 mAh/g) and a low practical energy density.[3,4] Moreover, the chemical diffusion coefficient of the lithium ion is always less than 10^{-6} cm^2/s in a graphite anode, which results in a low power density of the battery.[5]

Sn and Si have achieved much attention for their respective high theoretical capacities of 994 mAh/g and 4200 mAh/g. Compared to Si-based materials, SnO_2-based materials have advantages of lower price and easier processing for lithium-ion battery anodes.[6] However, both Sn and Si undergo significant volume expansion upon Li-insertion, which can be as high as 300%.[7] The volume expansion/contraction can result in cracking, which in turn leads to active material which is no longer in electrical contact with the remainder of the electrode and resultant poor cycle life and capacity fading.

Consequently, various efforts have been devoted to eliminate such a problem by applying different morphological schemes, example of which include, SnO_2 nanorods,[8] nanowires,[9,10] nanobelts,[11,12] nanotubes,[13,14] hollow spheres[15,16] and mesoporous structures.[17] The utilization of nanoparticles[18,19] seems to be a promising route to lessen the pulverization problem because it can reduce absolute local volume changes and also the diffusion path of lithium ions. Another

option is to introduce a suitable matrix, such as graphene,[20-23] TiO_2 nanofibers,[24] carbon nanofibers,[25] etc., to accommodate the volume change and to dissipate the local mechanical stress on SnO_2 nanoparticles.

Graphene, a single layer of carbon atoms arranged in a 2D honeycomb lattice, has superior electrical conductivity and a high surface area of over 2600 m^2/g.[26,27] As such, chemically reduced graphene oxide (rGO) has been investigated as a 2D conductive template on which SnO_2 nanoparticles are decorated to build a 3D interconnected porous network to improve the mechanical stability and Li^+ ions storage capacity.[20-23] Paek et al.[20] reported a charge capacity of 570 mAh/g at a current density of 100 mA/g after 30 cycles for SnO_2–graphene anode material prepared by the physical mixing of graphene nanosheets and SnO_2 nanoparticles. Zhu et al.[22] reported a discharge capacity of 649 mAh/g after 30 cycles at a current density of 50 mA/g for SnO_2–graphene, where the sample was prepared by a co-precipitation method. Long cycle life with superior charge–discharge capacities and rate capability of the SnO_2/graphene nanocomposites were not reported. Failure of these anode materials can be attributed to the inadequate dispersion of the SnO_2 nanoparticles on the graphene support. Most recently, Dimitrijevic et al. demonstrated theoretically that inter-particle spacing is an important design criterion for higher mechanical stability.[28] It was supported by experimental works[29,30] relating to void spaces acting as a buffer region for particle expansion. No report has been published on the evaluation of various microstructural changes based on SnO_2 content in the nanocomposite anode. An improved microstructure with highly dispersed nanoparticles may minimize volume expansion stress and avoid anode fracture. Moreover, SnO_2 nanoparticles tend to agglomerate with prolonged cycling which inevitably reduce the lithium storage capability as a result of hindered Li^+ ion diffusion and formation of unstable SEI.[31] Therefore, properly designed anode

architecture should be developed to minimize the aggregation of particles while keeping the electrode components highly conductive and active for electrochemical performance.

The present study is a systematic investigation of four different levels of SnO_2 content, i.e. 25, 43, 60, and 82 wt%, with various particle distributions on graphene support matrix. Correlation between the Li-ion cell performances and Sn/C ratio and microstructure of the SnO_2/graphene nanocomposites is investigated. The particle size and the corresponding inter-particle spacing were evaluated by transmission electron microscope imaging technique before and after cycling. The electrochemical performances were examined using multiple current density cycles.

2. Experimental

2.1. Materials

$SnCl_4.5H_2O$ (Tin(IV) chloride pentahydrate, Sigma-Aldrich, 98%), NaOH (Mallinckrodt Chemical Inc.), nano graphene platelet (N006-P, Angstron Materials Inc.), ethyl alcohol (Mallinckrodt Chemical Inc.) and Ar gas (ultra high purity grade, 99.99% Ar from Metro Welding Supply Corp.) were used as received without further purification.

2.2. Preparation of SnO_2/graphene nanocomposites

SnO_2 nanoparticles were synthesized by sol-gel method using $SnCl_4{\cdot}5H_2O$[32] as a precursor. 75 mL of a 0.1 M NaOH aqueous solution was added at a rate of 1 mL/min to an aqueous solution of $SnCl_4{\cdot}5H_2O$ (0.05 M, 150 mL) under vigorous stirring. The resultant light

white solution was sonicated (Branson 2510, 100 W) for 10 min. At the same time, two hundred mg of graphene nanoplatelets was mixed with ethylene glycol using an ultrasonic probe (Microson XL-2000, QSonica, LLC, 100 W) to make a dispersion with a concentration of 1 mg/mL. The dispersed graphene was added to the light white solution and stirred for three hours. The resulting solution was then centrifuged at 3000 rpm (Eppendorf International, Centrifuge 5804R) to collect the precipitate. The precipitate was washed with DI water and ethanol sequentially until the pH of the filtrate was close to 7. The solid product was dried under vacuum and heat treated at 400 °C for 2 h in an Ar atmosphere. Four different concentrations of SnO_2 in SnO_2/graphene, i.e., 25, 43, 60, and 82 wt%, were prepared.

2.3. Materials Characterization

Transmission electron microscopy (TEM) images were obtained using a JEOL JEM-2010 microscope. The samples were prepared by the dispersion of the materials in ethanol using sonication and drop-casting onto carbon-coated TEM grids and dried in air. Length of the particle diameter and the inter-particle distances were measured using AMT-600 from Advanced Microscopy Techniques Corp. A line connecting to the desired end points could give the linear measurement with a corresponding label. The morphology of these samples was also examined by scanning electron microscopy (SEM) using a JEOL JSM-7600F. Powder X-ray diffraction (XRD) was performed using a Rigaku SmartLab high resolution θ/2θ XRD system with a graphite monochromator with Cu Kα radiation (λ=1.5406 Å). Scattering angles (2θ) of 5-80° at a scanning rate of 3°/min was used. Thermogravimetric analysis (TGA) was conducted with a thermal gravimetric analyzer (TGA, Perkin Elmer Pyris-1) from 25 to 1000 °C at a rate of 10

°C/min under controlled airflow. The carbonaceous sample was burned in a TG furnace and the residue was Sn (IV) oxide.

2.4. Electrochemical tests

To fabricate an electrode, sample powder (SnO_2/Graphene) was mixed with 10 wt% conductive carbon (CNERGY Super C65, Timcal Graphite & Carbon) and pressed onto an expanded Cu microgrid (2Cu6-077F, Dexmet Corporation). The material was then assembled into test cells (#2032 coin cell) using lithium-metal foil as the negative electrode, a micro porous polypropylene separator (Celgard 2320), and an electrolyte of 1 M $LiPF_6$ in a 1:1(w/w) mixture of ethylene carbonate (EC) and dimethyl carbonate (DMC). Cells were assembled inside an argon filled glove box where both the moisture and oxygen content were below 1 ppm. All cells were tested at a constant current density of 100 mA/g between fixed voltage limits of 2V to 0.01V using a Maccor series 4200 battery tester. Moreover, the 25 wt% SnO_2/graphene sample was tested at 50 mA/g current density in a cycling test. The current density and electrode capacities were calculated based on the total mass of SnO_2 and graphene. Electrochemical impedance spectroscopy measurement was performed using a Gamry Reference 3000 from 1 MHz to 0.01 Hz at 3.5 mV rms.

3. Results and Discussion

3.1. TGA analysis

TGA was performed in air, in order to quantify the amount of SnO_2 in the nanocomposites. Fig. 1 shows the TGA profiles of different nanocomposite samples along with

pristine graphene and bare graphite (for comparison). SnO_2 mass percent is determined to be about 82, 60, 43, and 25% respectively in four different samples of SnO_2/graphene nanocomposites. The pristine graphene and graphite had the greatest weight loss at 620°C and 710 °C, respectively, and the composites were stable until 680°C. These results are consistent with previous reports.[33-35] Weight loss of graphene at a temperature as low as 200°C is attributed to pyrolysis of the labile oxygen-containing functional groups such as OH, COOH, etc.[36] However, this low temperature weight loss was not observed for SnO_2/graphene materials because these functional groups were removed during the nanocomposite synthesis process.

3.2. Microstructure characterization

3.2.1. SEM observations

The morphology and structural features of the SnO_2/graphene nanocomposites were studied by scanning electron microscopy (SEM), transmission electron microscopy (TEM) and energy-dispersive X-ray spectroscopy (EDS) analyses. Figs. 2(a), 2(b), 2(c), and 2(d) present the corresponding SEM images of the SnO_2/graphene nanocomposites with different SnO_2 nanoparticle concentrations of 82, 60, 43, and 25 wt%, respectively. Microstructural changes can clearly be observed while changing the SnO_2 content in the composites. Micron-sized agglomerated SnO_2 particles are evident for the 82 and 60 wt% (Figs. 2(a) and (b)) composites, which are not attached to the graphene sheets. Whereas, in the 43 wt% composite (Fig. 2(c)), few numbers of nanometer scale clusters of the particles are obvious. No visible cluster of the nanoparticles can be identified for the 25 wt% composite (Fig. 2(d)). A uniform distribution of the SnO_2 nanoparticles in the 2D graphene matrix with substantial void spaces is observed for the 25 wt% SnO_2/graphene nanocomposite (Fig. 2(e)).

3.2.2. TEM observations

High magnification HRTEM images (Figs. 3(a), (b), (c), and (d)) of all four samples reveal the distribution of SnO_2 nanoparticles on the graphene sheets. The average particle size (based on 40 – 100 counts per material) of SnO_2 was determined to be $6.78 \pm 0.4 > 5.55 \pm 0.5 > 3.87 \pm 0.2 > 1.9 \pm 0.1$ nm for 25, 43, 60, and 82 wt% composites, respectively. The inter-particle distances are measured as 1.8 ± 0.1 and 2.19 ± 0.33 nm for 25 and 43 wt% nanocomposites, respectively. The difference in the inter-particle distances between the 25 wt% and 43 wt% samples can be attributed to particle size and agglomeration. The accurate inter-particle distances couldn't be measured for 60 and 82 wt% composites, as the particles are agglomerated and closely attached to each other. Dimitrijevic et al.[28] predicted by modeling that cracking damages during Li-insertion can be minimized by keeping the interparticle spacings at least 1.5 times their diameter. However, their calculations was based on the periodical occupation of spherical Sn with 3D matrix. Hence, the interparticle distances are decreased in the order of 25 > 43 > 60 and 82 wt% composites compared to their particle diameters. Based on Fig. 3(d), 25 wt% composite is showing the nanoparticles are spaced adequately apart from each other. This particular microstructure minimizes the mechanical instability which refers to the microcracking/crumbling of the alloy material for Li^+ insertion/removal during charging/discharging.[37] In 60 and 82 wt% SnO_2 samples (Figs. 2 (a), (b) and 3 (a), (b)), it is seen that nanoparticles are agglomerated into bigger clusters of few nm to micron sized and these particles are anticipated to be freestanding rather than attached to the matrix (graphene sheets). When the loading of SnO_2 is decreased to 43 and 25 wt%, the uniformly dispersed nanoparticles are attached on the surface of graphene sheets (Figs. 3(c) and (d)). These findings indicated that only when the contents of SnO_2 is

reduced to 25 wt%, good dispersion of SnO_2 nanoparticles with optimum inter-particle distances occurred.

3.2.3. XRD analysis

To identify the crystalline structure, the XRD pattern of the as-prepared nanocomposite powder was investigated (Fig. 4). The diffraction peaks at around 27, 34, 52, and 66° are assigned to the index numbers of SnO_2 (110), (101), (211), and (301), respectively. No impurity diffraction peaks due to metallic Sn or other tin oxides are present. These peaks are in good agreement with the tetragonal rutile structure of SnO_2 particles which present as cassiterite following the reference pattern JCPDS 41-1445. In the XRD pattern, the progressively broadened diffraction peaks with lowering the SnO_2 content from 82 to 25 wt% are due to the smaller grain sized particles in the samples. The Scherrer formula was used to calculate the crystal size of the SnO_2 particles: $d = 0.9\lambda/(\beta\cos\theta)$, where λ is the x-ray wavelength, β is the full width at half maximum intensity, and θ is the angle corresponding to the peak. Using the Scherrer equation for the (101) peak ($2\theta = 34°$), the sizes of SnO_2 crystals in the 25, 43, 60, and 82 wt% SnO_2 are 4, 8, 11, and 12 nm, respectively. Average particle sizes were calculated based on Scherrer equation which includes contributions from grains and agglomerates. Hence, from the TEM images and the XRD patterns, the individual particle sizes are around 2-3, 4-8, 6-11, and 7-12 nm for 25, 43, 60, and 82 wt% composites, respectively. The larger SnO_2 nanoparticles with higher Sn/C ratios are attributed to the higher initial Sn^{4+} ion concentrations in the precursors.[38] The major diffraction peak is at ~27° (002) for graphene platelets which is located in the same peak position of SnO_2 (110) in the SnO_2/graphene nanocomposites.

3.3. Electrochemical characterization

To evaluate the storage capacity and cyclability, the 25, 43, 60, and 82 wt% SnO_2/graphene nanocomposites were used as cathodes for lithium ion half-cell configurations with respect to 'Li' as anodes. Fig. 5 (a) shows the galvanostatic first cycle charge-discharge profiles for the anodes measured at a current density of 100 mA/g and cutoff voltage range of 0.01 V - 2.0 V. In the first discharging (Li insertion) process, all samples show plateau at around 1.0 V- 0.8 V, which is also observed for the graphene anode. The plateau can be attributed to the formation of solid-electrolyte interface (SEI) and Li_2O and Sn according to the reaction: $SnO_2 + 4Li \rightarrow Sn + 2Li_2O$.[39] This plateau becomes progressively smaller when the loading of SnO_2 decreased from 82 to 25 wt%, indicating that Li_2O is formed in smaller quantities as a result of lower loading of SnO_2 in the nanocomposites. This plateau nearly disappeared from the second cycle for only the 25 wt% sample, which suggests that there is lower first cycles irreversible capacity losses with well dispersed SnO_2 nanoparticles in the nanocomposite. For charge cycles, the SnO_2-graphene nanocomposites showed a plateau at around 0.5 V due to the reaction: $Li_xSn \leftrightarrow Sn + xLi^+ + xe^-$ ($0 \leq x \leq 4.4$) with the maximum 4.4 Li insertion for one Sn for the formation of $Li_{22}Sn_5$ alloy.[40,41] Lithium can intercalate with graphite according to the reaction: $Li^+ + 6C + e^- \leftrightarrow LiC_6$.[42] The lithium intercalation/deintercalation potential in the graphene layers of graphite is ~0.2-0.1 V.[43] The potential plateaus at around ~ 0.1 V become progressively larger with the lower SnO_2 content in the composites. This observation implies that the synergistic effect of both SnO_2 and pristine graphene is enhanced with proper morphology of SnO_2 nanoparticles and good dispersion on the graphene sheets.

A comparative study of specific capacities with cycling of four nanocomposites, pure SnO_2 nanopowder and pristine graphene are shown in Fig. 5(b). In the first cycle at a current

density of 100 mA/g, the anode materials deliver the lithium insertion capacity (the discharge cycle) of 1730, 1310, 1200, 1044, 595, and 1461 mAh/g for the 82, 60, 43, 25 wt% SnO_2/graphene nanocomposites, pristine graphene, and pure SnO_2 nanopowder, respectively. Theoretical capacity of SnO_2 for the first cycle lithium insertion process is 1494 mAh/g.[22,39] It is well-known that in the initial cycle, the irreversible capacities of lithium ion batteries are mainly caused by the formation of solid electrolyte interphase (SEI) films, as a result of the irreversible reactions of lithium ions with electrolyte species. SEI films have the permeability for lithium ions and protect the electrode surface from further reactions with electrolytes.[39,44] The first cycle irreversible reaction to form Sn and Li_2O from Li^+ and SnO_2 is also responsible for the capacity loss.[40,41] After 30 cycles, pure SnO_2 nanopowder electrode (Fig. 5b) exhibits a rapidly decayed discharge capacity of 178 mAh/g (12% retention of the initial capacity), whereas pristine graphene exhibits stable capacity of 375 mAh/g (63% retention of the initial capacity). The main reason of rapid capacity fading for pure SnO_2 nanoparticles is the large volume expansion of Sn during alloying reaction with lithium, leading to pulverization of the electrode.[21,23] The 82 wt% composite exhibited similar trend of early cycle decay as the pure SnO_2 nanoparticles. Though the 60 wt% composite exhibits better capacity retention in the early cycles, after 30 cycles the capacity retention is very low (only 183 mAh/g, 14% of initial capacity). Based on the results for the pristine graphene and pure SnO_2 electrodes, the cycling instability is attributed to the diminishing electrochemical activity of the Sn particles. Hence, graphene matrix alone cannot provide sufficient stabilizing effect to the composites with higher Sn content.

For the 43 wt% composite, an improvement to the capacity retention is observed compared to 60 and 82 wt% composites, with a reversible capacity of 400 mAh/g and slower

fading rate of 1.1% after 30 cycles, compared to 5.2 and 4.1% for 82 and 60 wt% composites, respectively. This improvement of cycling stability with higher capacity is likely due to the smaller size and better dispersion of nanoparticles on the graphene sheets. However, the average inter-particle distance is about 2.2 nm for these 4-8 nm diameter SnO_2 particles, which still cannot provide the sufficient spacing and dispersion for good structural stability with cycling.

Further improvement of the capacity retention is observed for the 25 wt% SnO_2 composite (Figs. 5 and 6). The discharge capacity is 662 mAh/g after 150 cycles and 640 mAh/g after 30 cycles at 50 and 100 mA/g current densities, respectively. The theoretical capacity of 25 wt% SnO_2/graphene was calculated to be 753.5 mAh/g based on the theoretical capacity of SnO_2 (782 mAh/g) and pristine graphene (744 mAh/g)[45]. The observed capacities of 25 wt% SnO_2/graphene are comparable to the theoretical capacity, suggesting that there are synergistic effects to improve cyclic performance. This distinct performance can be attributed to the microstructure optimization of the composite. SEM and TEM images (Figs. 2 and 3) reveal that graphene sheets are well-separated and SnO_2 nanoparticles are highly dispersed on the matrix. The average diameter of SnO_2 nanoparticle is around 2-3 nm with ~2 nm inter-particle spacing. With this particle size and spacing, SnO_2 nanoparticles can react with lithium without developing excessive internal stress and form a stable SEI layer on the surface of the particles.[46,47] Better dispersion can lead to the less re-stacking of the graphene nanosheets with cycling which can act as a better lithium storage electrodes.[21,23] Furthermore, well-dispersion can enhance the benefits of conductive graphene network in the electrode. Hence, well-distributed nanoparticles on graphene should exhibit stronger synergistic effects of both graphene and Sn nanoparticles with enhanced capacity retentions. Although at 50 mAh/g current density, the 25 wt% composite

shows higher discharge capacity 662 mAh/g after 150 cycles with high coulombic efficiency of 95%, a slow capacity fading with cycling is still evident as seen in Fig. 6 (a). This suggested that at this smaller current density, 2 nm sized particles with very high surface area can increase the surface interactions with the electrolyte; such instances may result in the unwanted side reactions, forming an insulating and Li^+ impeding layers, which may affect the corresponding anode cyclic performances.[48,49]

To further elucidate the effects of microstructural improvement to the electrochemical performance of the 25 wt% SnO_2/graphene electrode, the rate capabilities were evaluated at different current densities, as shown in Fig. 6 (b). The discharge capacity of the 25 wt% SnO_2/graphene electrode decreases as the current density increases, and the electrode shows a stable specific capacity of 525 mAh/g at a current density of 300 mA/g and 445 mAh/g at a current density of 500 mA/g. These results are much more promising than the previous studies.[20-23] When the current density reaches 1000 mA/g, the capacity becomes stable at 230 mAh/g. After cycling at high current densities, the cell is galvanostatically discharged/charged again at a current density of 300 mA/g, and substantial capacity is recovered without noticeable capacity fading. This result indicates a fully preserved microstructure of the nanocomposite electrode after cycling even at higher current rates.

3.4. TEM observations after cycling

The TEM images in Figs. 7 (a) and (b) show the 82 and 25 wt% SnO_2/graphene nanocomposites in the de-lithiated condition after 100 charge-discharge cycles. Large Sn nanoclusters (>15 nm) on graphene nanosheets for the 82 wt% sample are evident, compared

with around 7 nm before cycling (Fig. 3). This can be attributed to aggregation of Sn on the graphene nanosheets upon cycling. On the other hand, for the 25 wt% sample, Sn nanoparticles are well-spread out on the graphene sheets and retained a size of around 3 nm after cycling, which is comparable to the original particle size. Furthermore, in Fig. 7(a), larger and agglomerated Sn particles are pulverized to several nano- and micron-sized particles for 82 wt% loading, whereas, in Fig. 7(b), nano-sized particle distribution was observed for 25 wt% electrodes without any pulverization.[30] Fig. 8 is the schematic representation of four SnO_2/graphene composites before and after cycling. After cycling, the 82 (Fig. 7(a)) composite has more agglomerated and larger particles than the 25 wt% (Fig. 7(b)) composite and micron-sized Sn-clusters are surrounded by nano-sized particles.[18] The least particle expansion with stable inter-particle distances can be observed for the 25 wt% SnO_2/graphene composite after the electrochemical cycles.

3.5. Impedance spectroscopy analysis

Fig. 9 shows the AC impedance spectroscopy (EIS) for 25 and 82 wt% SnO_2/graphene electrodes before cycling and after 100 cycles, along with the equivalent circuit model (inset). In these Nyquist plots, the intercept at the Zreal axis corresponds to the solution resistance (R_s), which represents uncompensated total resistance of the electrolyte, separator and electrical contacts. The diameter of the semicircle in the high to middle frequency region includes the superposition of the impacts of the surface films (resistance to Li^+ ion migration) and the charge transfer resistance (R_{ct}) coupled with the relevant double layer capacitance (constant phase element (CPE).[50] The inclined line at lower frequencies represents the Warburg impedance (W),

which is associated with lithium ion diffusion in the SnO_2/graphene nanoparticles. There is very little difference among the R_s values (6-14 Ω) of all four composites before and after cycling. R_{ct} values are listed in Table 1 for the composites at different cycles. It can be seen that there is an increase in the value of R_{ct} with cycling for 82 and 60 wt% composites, which can be attributed to the increase in the inter-particle contact resistance induced by continuous SEI formation on the particles during cycling.[50] Moreover, the increase in R_{ct} as wt% of SnO_2 increases could be due to the higher degree of agglomeration and lack of homogeneity in the electrode resulting in poor electric contact.[51] On the other hand, for the 43 and 25 wt% composites, R_{ct} values decrease with cycling which can be mainly ascribed to an enhanced electron and Li^+ ion transport for well-dispersed SnO_2 nanoparticles on the graphene sheets which facilitates a stable passive layer formation on the nanoparticles.[35] The higher graphene content with the same amount of carbon black could increase the conductivity resulting in the lower R_{ct}.

4. Conclusions

The Sn/C ratio and microstructure of SnO_2/graphene nanocomposite anode can dramatically affect the electrochemical properties of Li-ion batteries. Optimized anode structure was obtained for 25/75 wt% SnO_2/graphene composite containing 2-3 nm SnO_2 nanoparticles with ~2 nm inter-particle distance, which noticeably enhanced the electrochemical properties of SnO_2/graphene composite anodes. The excellent discharge capacity retention and rate capability of 25/75 wt% SnO_2/graphene composite compared to higher Sn contents may be attributed to: i) optimal particle size ii) well-distributed nanoparticles with good inter-particle distance, iii) formation of stable electrode-electrolyte interface during cycling, and iv) increased synergistic effects of both graphene and SnO_2.

Acknowledgement

Financial support from the Department of Energy (Grant DE-EE0002106) for this research is gratefully acknowledged.

References

(1) H. Buqa, D. G., M. Holzapfel, M. E. Spahr, P. Novak, *J. Electrochem. Soc.* **2005**, *152*, A474.

(2) Y.P. Wu, E. R., R. Holze, *J. Power Sources* **2003** *114*, 228.

(3) J.R. Dahn, Z. T., Y. Liu, J.S. Xue, *Science* **1995** *270*, 590.

(4) K. Sato, M. N., A. Demachi, N. Oki, M. Endo, *Science* **1994** *264*, 556.

(5) K. Persson, V. A. S., L. J. Hardwick, Y. Hinuma, Y. S. Meng, A.V.D. Ven, V. Srinivasan, R. Kostecki, G. Ceder, *J. Phys. Chem. Lett.* **2010**, *1*, 1176.

(6) A.R. Kamali, D. J. F., *Rev.Adv.Mater.Sci.* **2011**, *27*, 14.

(7) L.Y. Beaulieu, K. W. E., R.L. Turner, L. J. Krause, J.R. Dahn, *Electrochem.Solid-State Lett.* **2001**, *4*, A137.

(8) X. Ji, X. H., J. Liu, J. Jiang, X. Li, R. Ding,Y,.Hu, F. Wu, Q Li, *Nanoscale Res Lett.* **2010**, *5*, 649.

(9) P. Meduri, C. P., V. Kumar, G. U. Sumanasekera, M. K. Sunkara, *Nano Lett.* **2009**, *9*, 612.

(10) M. Park, G. W., Y. Kang, D. Wexler, S. Dou, H. Liu, *Angew. Chem.* **2007**, *119*, 764

(11) J. Hu, Y. B., Q. Liu, D. Golberg, *Adv. Funct. Mater.* **2003**, *13*, 493.

(12) J. Duan, S. Y., H. Liu, J. Gong, H. Huang, X. Zhao, R. Zhang, Y. Du, *J. Am. Chem. Soc.* **2005**, *127*, 6180.

(13) J. Ye, H. Z., R. Yang, X. Li, L. Qi, *small* **2010**, *6*, 296.

(14) Y. Jia, L. H., Z. Guo, X. Chen, F. Meng, T. Luo, M. Li, J. Liu, *J. Phys. Chem. C* **2009**, *113*, 9581.

(15) J. Yu, H. G., S. A. Davis, S. Mann, *Adv. Funct. Mater.* **2006**, *16*, 2035.

(16) X. W. Lou, Y. W., C. Yuan, J. Y. Lee, L. A. Archer, *Adv. Mater.* **2006**, *18*, 2325.

(17) X. Wang, Z. L., Q. Li, C. Wang, A. Chen, Z. Zhang, R. Fan, L. Yin, *Cryst. Eng. Comm.* **2013**, *15*, 3696.

(18) C. Kim, M. N., M. Choi, J. Cho, B. Park, *Chem. Mater.* **2005**, *17*, 3297.

(19) J. Hassoun, G. D., S. Panero, B. Scrosati, *Adv. Mater.* **2008**, *20*, 3169.

(20) S. M. Paek, E. Y., I. Honma, *Nano Lett.* **2009**, *9*, 72.

(21) J. Liang, W. W., D. Zhong, Q. Yang, D. L. Li, L. Guo, *ACS Appl. Mater. Interfaces* **2012**, *4*, 454.

(22) X. Zhu, W. Y. Z., S. Murali, D. M. Stoller, S.R. Ruoff, *J. Power Sources* **2011**, *196*, 6473.

(23) H. Kim, W. S. K., U. Y. Park, H. Gwon, H. D. Seo, Y. Kim, K. Kang, *Nano Res.* **2010**, *3*, 813.

(24) Toan Tran, K. M., Jianlin Li, Zhonghe Bi, Ji Wu, *Electrochimica Acta* **2014**, *117*, 68.

(25) Christopher A. Bonino, L. J., Zhan Lin, Ozan, Toprakci, Xiangwu Zhang, Saad A. Khan, *ACS Appl. Mater. Interfaces* **2011**, *3*, 2534.

(26) Y. Hernandez, V. N., M. Lotya, F.M .Blighe, Z. Sun, S. De, I.T. McGovern, B. Holland, M. Byrne, Y.K. Gun'Ko, J.J. Boland, P. Niraj, G. Duesberg, S. Krishnamurthy, R. Goodhue, J. Hutchison, V. Scardaci, A.C. Ferrari, J.N. Coleman, *NatNanotechnol* **2008**, *3*, 563.

(27) F. Banhart, P. M. A., *Nature* **1996**, *382*, 433.

(28) B. J. Dimitrijevic , K. E. A., K. Hackl, *J Power Sources* **2012**, *206*, 343.

(29) N. Liu, H. W., M. T. McDowell, Y. Yao, C. Wang, Y. Cui, *Nano Lett.* **2012**, *12*, 3315.

(30) K. E. Aifantis, M. H., P. Sanders, S. A. Hackney, *Mater Sci Eng A* **2011**, *529*, 55.

(31) Q. Zhang, E. U., S. L. Candelaria, G. Cao, *Chem. Soc. Rev.* **2013**, *42*, 3127.

(32) L. Korosi, K. M., R. Kun, J. Nemeth, I. Dekany, *Progr Colloid Polym Sci.* **2004**, *125*, 27.

(33) M. Wojtoniszak, X. C., R.J. Kalenczuk, A. Wajda, J. Łapczuk, M. Kurzewski, M. Drozdzik, P.K. Chu, E. Borowiak-Palen, *Colloids Surf. B* **2012**, *89*, 79.

(34) Y. Chen, H. Z., L. Sheng, L. Yu, K. An, J. Xu, Y. Ando, X. Zhao, *Chem. Phys. Lett.* **2012**, *538*, 72.

(35) B. Wang, D. S., J. Park, H. Ahn, G. Wang, *Nanoscale Res. Lett.* **2012**, *7*, 215.

(36) S. Stankovich, D. A. D., R. D. Piner, K. A. Kohlhaas, A. Kleinhammes, Y. Jia, Y. Wu, S. T. Nguyen, R. S. Ruoff, *Carbon* **2007**, *45*, 1558.

(37) K. E. Aifantis, S. A. H., J. P. Dempsey, *J. Power Sources* **2007**, *165*, 874.

(38) Caue Ribeiro, E. J. H. L., Tania R. Giraldi, Elson Longo, Jose´ A. Varela, Edson R. Leite, *J. Phys. Chem. B* **2004**, *108*, 15612.

(39) I.A. Courtney, J. R. D., *J. Electrochem.Soc.* **1997**, *144*, 2045.

(40) M. Winter, J. O. B., M. Spahr, P. Novak, *Adv. Mater.* **1998**, *10*, 725.

(41) M. Winter, J. O. B., *Electrochim. Acta* **1999**, *45*, 31.

(42) K. Tatsumi, N. I., H. Sakaebe, H. Shioyama, S. Higuchi, *J. Electrochem.Soc.* **1995**, *142* 716.

(43) J. R. Dahn, *Phys. Rev. B* **1991**, *44*, 9170.

(44) D. Aurbach, A. Z., Y. Ein-Eli, I. Weissman, O. Chusid, B. Markovsky, *J Power Sources* **1997**, *68*, 91.

(45) G. Wang, B. W., X. Wang, J. Park, S. Dou, H. Ahnb, K. Kim, *J. Mater. Chem.* **2009**, *19*, 8378.

(46) D. Aurbach, B. M., I. Weissman, E. Levi, Y. Ein-Eli, *Electrochim. Acta* **1999**, *45*, 67.

(47) B. Guo, J. S., K. Tang, Y. Bai, Z. Wang, L. Chen, *J. Power Sources* **2008**, *177*, 205.

(48) J. Chen, *Materials* **2013**, *6*, 156.

(49) M. J. Armstrong, C. O. D., W. J. Macklin, J. D. Holmes, *Nano Res.* **2013**.

(50) Z. P. Guo, Z. W. Z., H.K. Liu, S. X. Dou, *Carbon* **2005**, *43*, 1392.

(51) J. Li, B. L. A., J. Kiggans, C. Daniel, D L. Wood, *Journal of The Electrochemical Society* **2013**, *160* A201.

Table

Table 1. AC impedance spectroscopy results of the charge transfer resistance (R_{ct}) values of 82, 60, 43 and 25 wt% SnO_2/graphene nanocomposite electrodes.

SnO_2/Graphene Electrodes	**R_{ct} (Ω)**	
	Before cycling	**After 100 cycles**
82 wt%	316	498
60 wt%	250	394
43 wt%	230	132
25 wt%	240	126

List of Figure Captions

Fig. 1 TGA curves of different SnO_2/graphene composite with 82, 60, 43, and 25 wt % SnO_2, pristine graphene nanosheets and graphite.

Fig. 2 SEM images of (a) 82, (b) 60, (c) 43, and (d) lower magnification and (e) higher magnification of 25 wt% SnO_2 concentrations in SnO_2/Graphene composites.

Fig. 3 TEM images of SnO_2/Graphene composite with (a) 82, (b) 60, (c) 43, and (d) 25 wt% SnO_2. Yellow lines are indicating the length of the nanoparticles and aqua colored lines are the measurement of inter-particle distances.

Fig. 4 XRD pattern of the SnO_2/graphene nanocomposite for 82, 60, 43, and 25 wt% SnO_2 and pristine graphene nanosheets.

Fig. 5 (a) Galvanostatic charge-discharge profile for first and second (dotted line) cycle and (b) cyclic performance at a current density of 100 mA/g for the samples of 82, 60, 43, and 25 wt% SnO_2 in the composites, SnO_2 nanopowders, and pristine graphene nanosheets.

Fig. 6 (a) Galvanostatic charge-discharge profile for different cycles in inset and cyclic performance at a current density of 50 mA/g, (b) rate capability study of 25 wt% SnO_2/graphene nanocomposite.

Fig. 7 TEM images of (a) 82 and (b) 25 wt% SnO_2/graphene after 100 discharge/charge cycles.

Fig. 8 Schematic illustrations of 82, 60, 43, and 25 wt% SnO_2/graphene nanocomposites before and after electrochemical cycling.

Fig. 9 Nyquist plots of 82 and 25 wt% SnO_2/graphene anodes before and after 100 discharge/charge cycles.

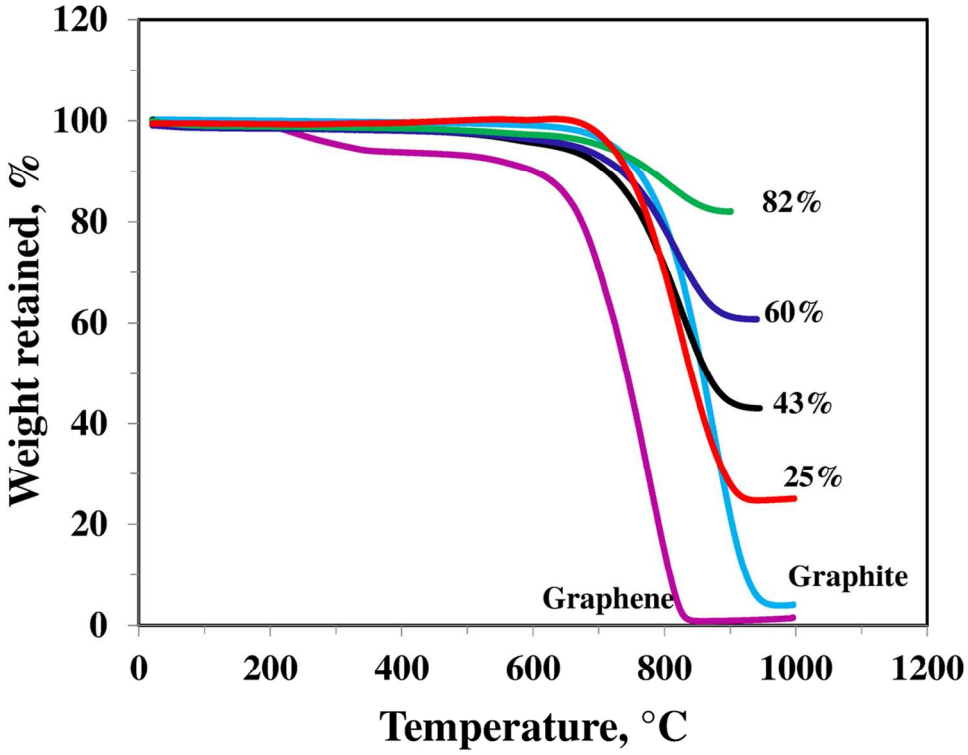

Figure 1. TGA curves of different SnO2/graphene composite with 82, 60, 43, and 25 wt % SnO2, pristine graphene nanosheets and graphite.
112x89mm (300 x 300 DPI)

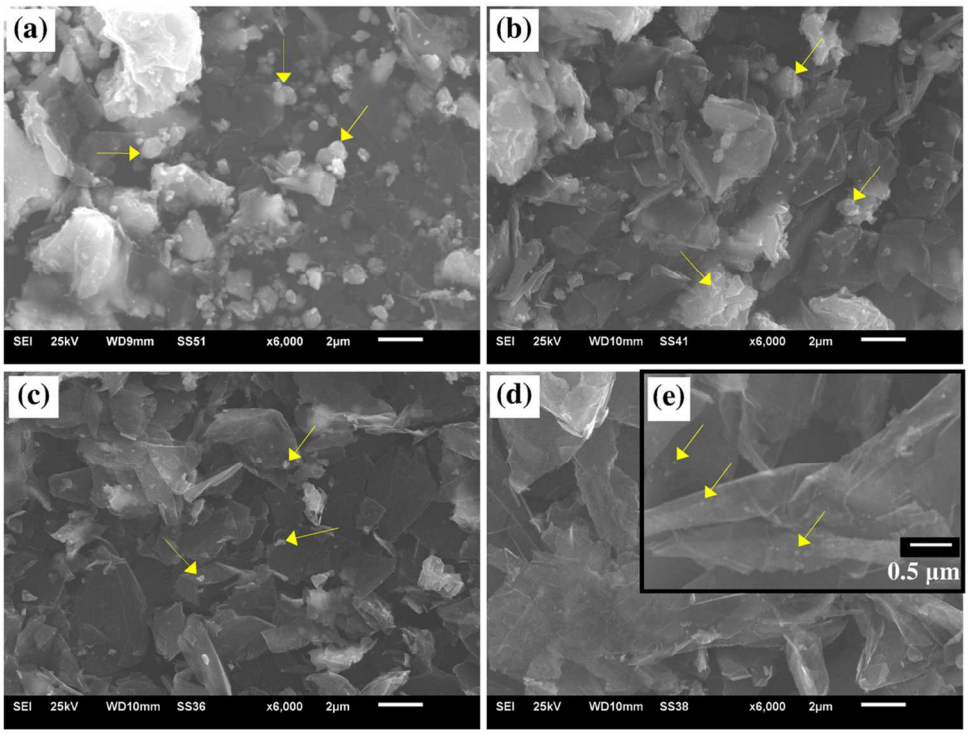

Figure 2. SEM images of (a) 82, (b) 60, (c) 43, and (d) lower magnification and (e) higher magnification of 25 wt% SnO2 concentrations in SnO2/Graphene composites.
104x79mm (300 x 300 DPI)

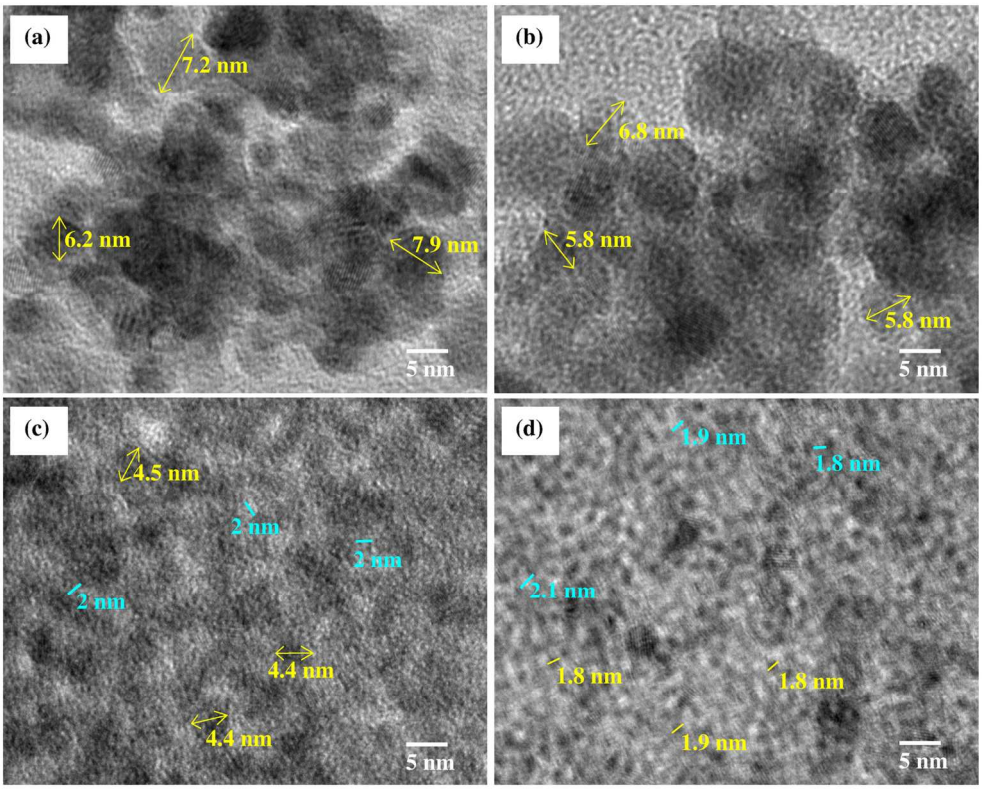

Figure 3. TEM images of SnO2/Graphene composite with (a) 82, (b) 60, (c) 43, and (d) 25 wt% SnO2. Yellow lines are indicating the length of the nanoparticles and aqua colored lines are the measurement of inter-particle distances.
143x115mm (300 x 300 DPI)

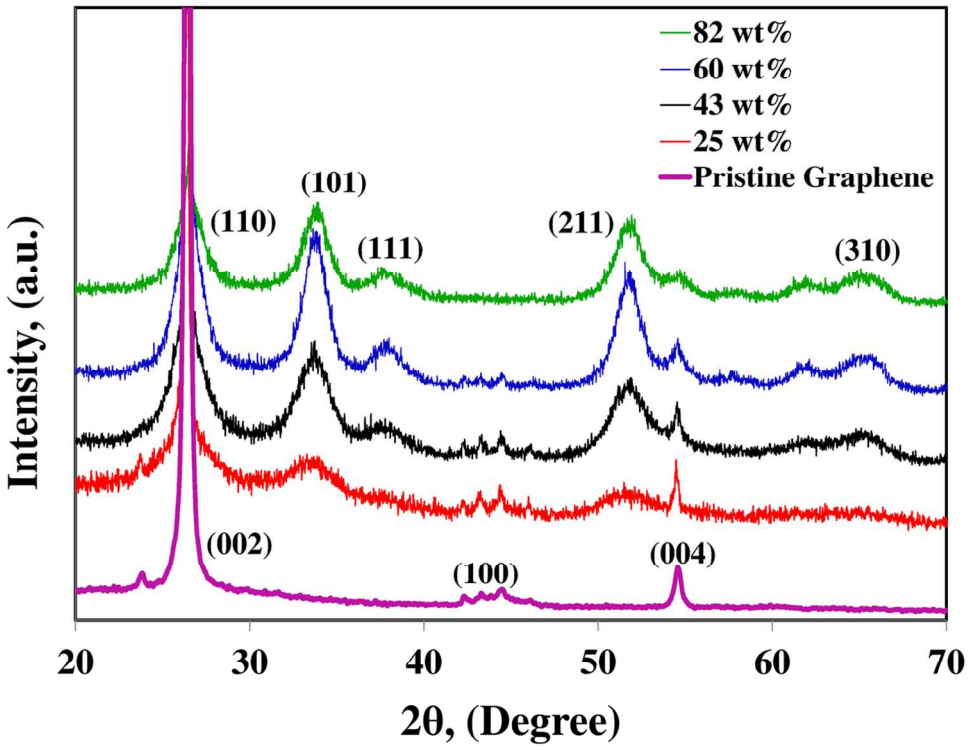

Figure 4. XRD pattern of the SnO2/graphene nanocomposite for 82, 60, 43, and 25 wt% SnO2 and pristine graphene nanosheets.
110x86mm (300 x 300 DPI)

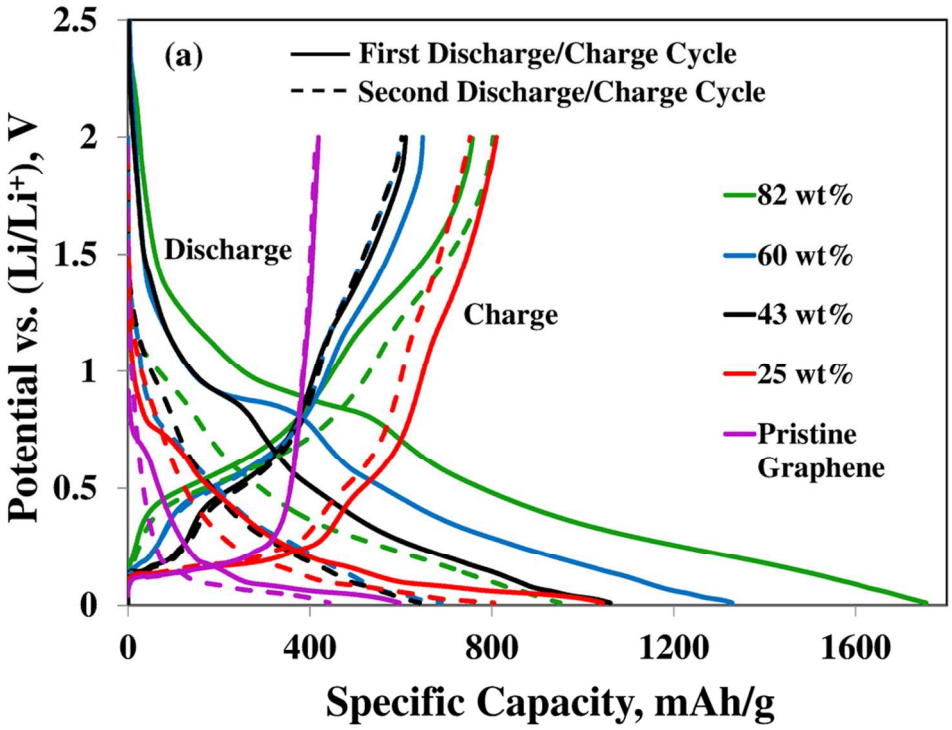

Figure 5. (a)Galvanostatic charge-discharge profile for first and second (dotted line) cycle at a current density of 100 mA/g for the samples of 82, 60, 43, and 25 wt% SnO2 in the composites, SnO2 nanopowders, and pristine graphene nanosheets.
92x70mm (300 x 300 DPI)

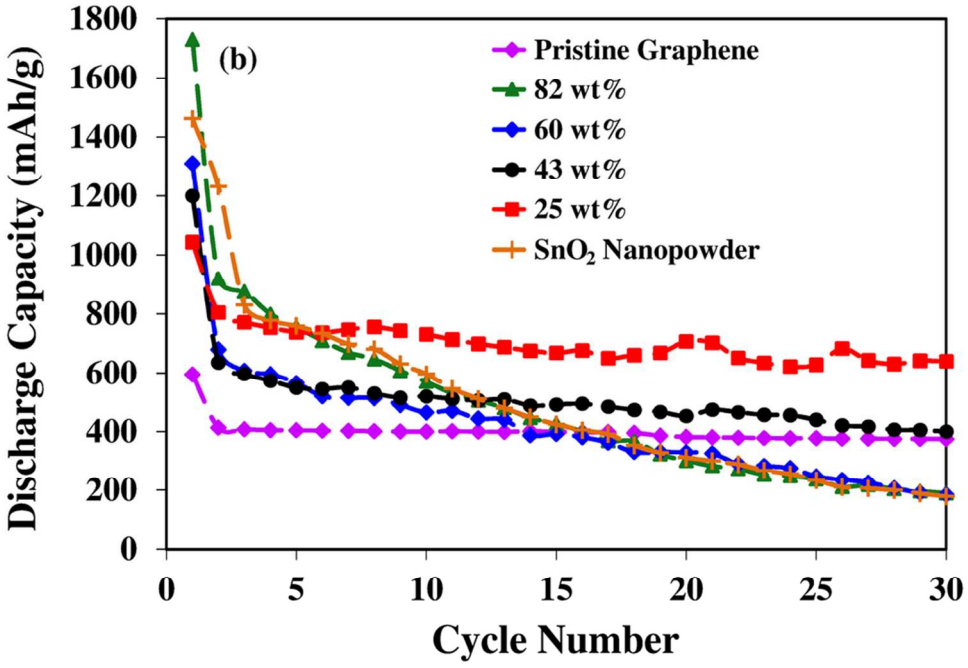

Figure 5. (b)Cyclic performance at a current density of 100 mA/g for the samples of 82, 60, 43, and 25 wt% SnO2 in the composites, SnO2 nanopowders, and pristine graphene nanosheets.
88x61mm (300 x 300 DPI)

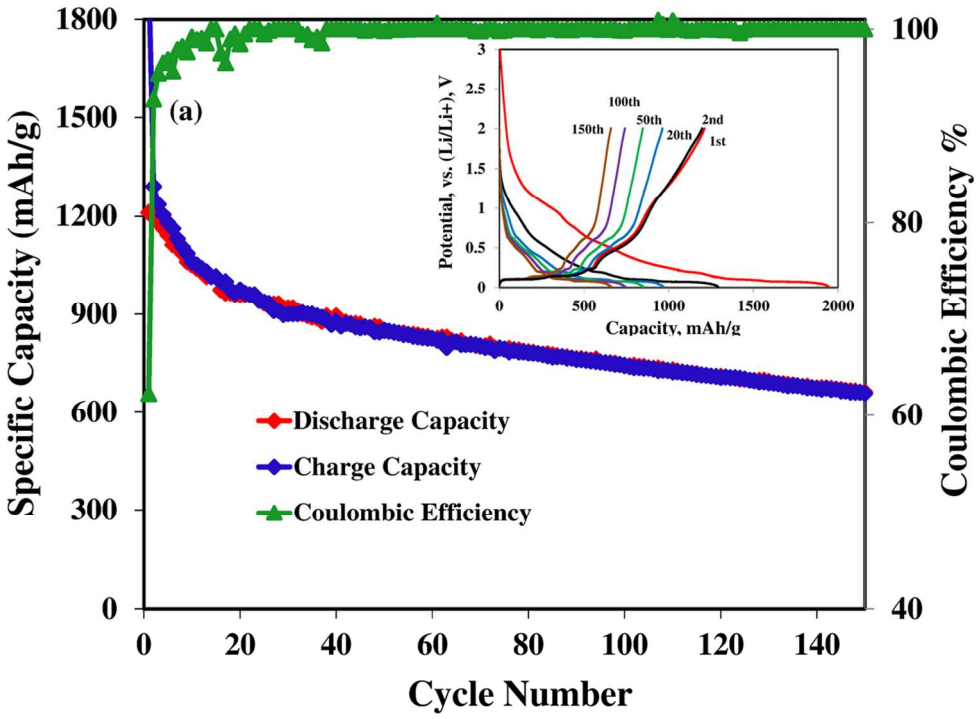

Figure 6. (a) Galvanostatic charge-discharge profile for different cycles in inset and cyclic performance at a current density of 50 mA/g of 25 wt% SnO2/graphene nanocomposite.
105x78mm (300 x 300 DPI)

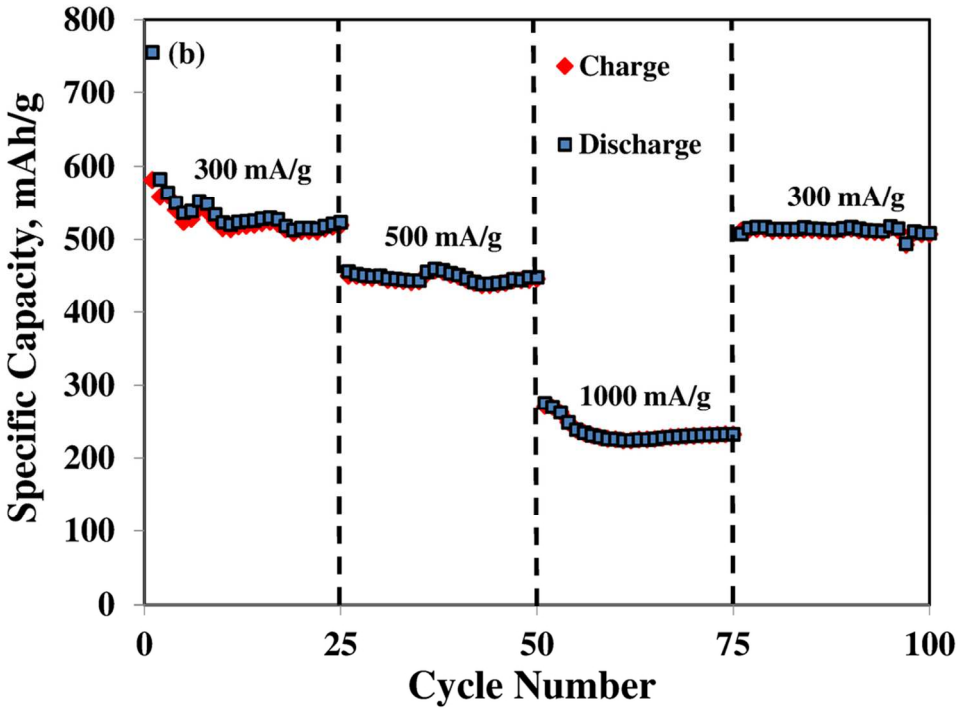

Figure 6. (b) Rate capability study of 25 wt% SnO2/graphene nanocomposite.
97x72mm (300 x 300 DPI)

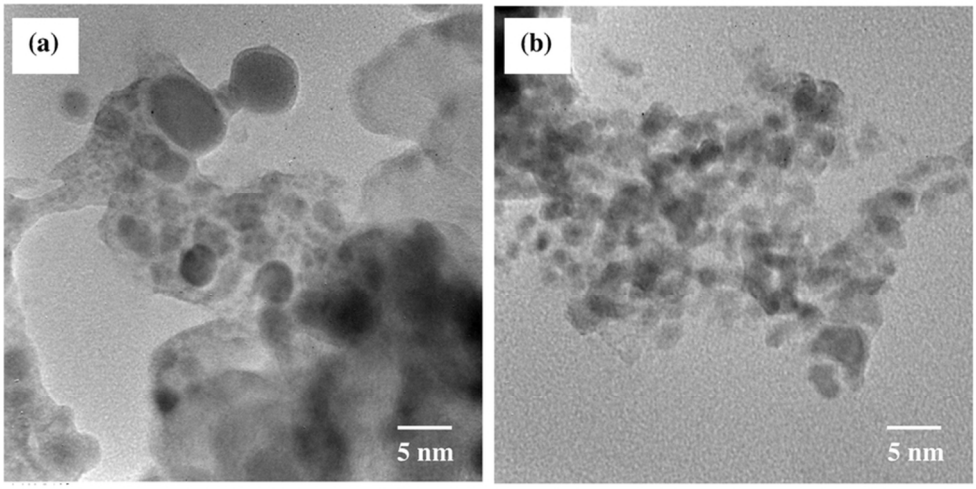

Figure 7. TEM images of (a) 82 and (b) 25 wt% SnO2/graphene after 100 discharge/charge cycles.
78x39mm (300 x 300 DPI)

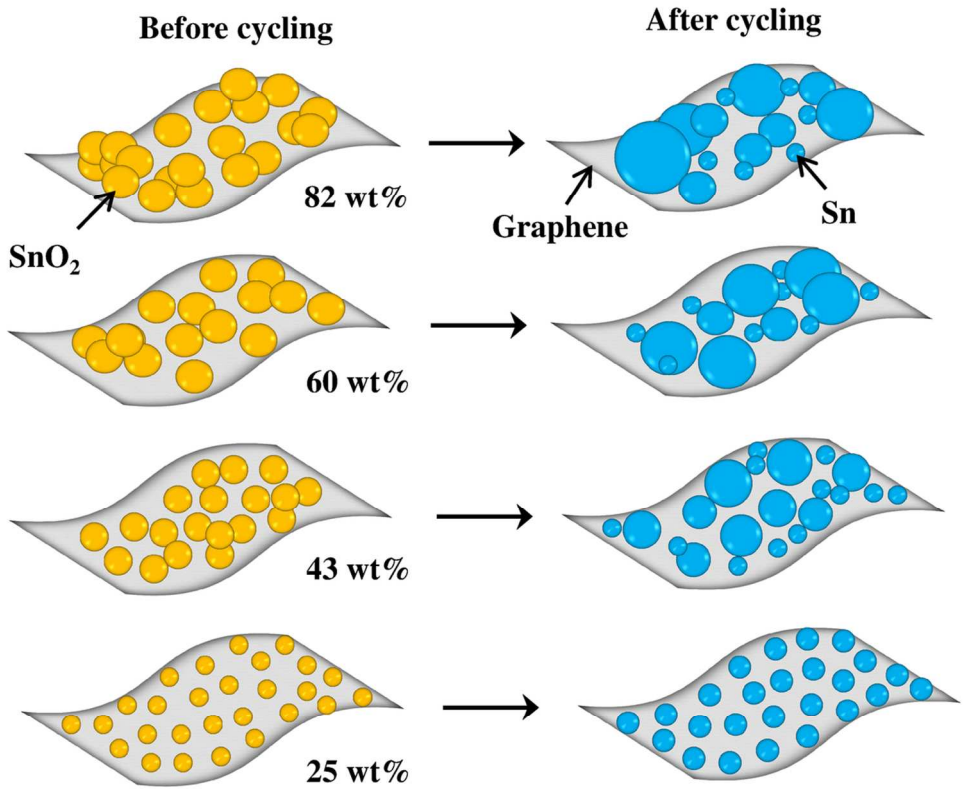

Figure 8. Schematic illustrations of 82, 60, 43, and 25 wt% SnO2/graphene nanocomposites before and after electrochemical cycling.
107x89mm (300 x 300 DPI)

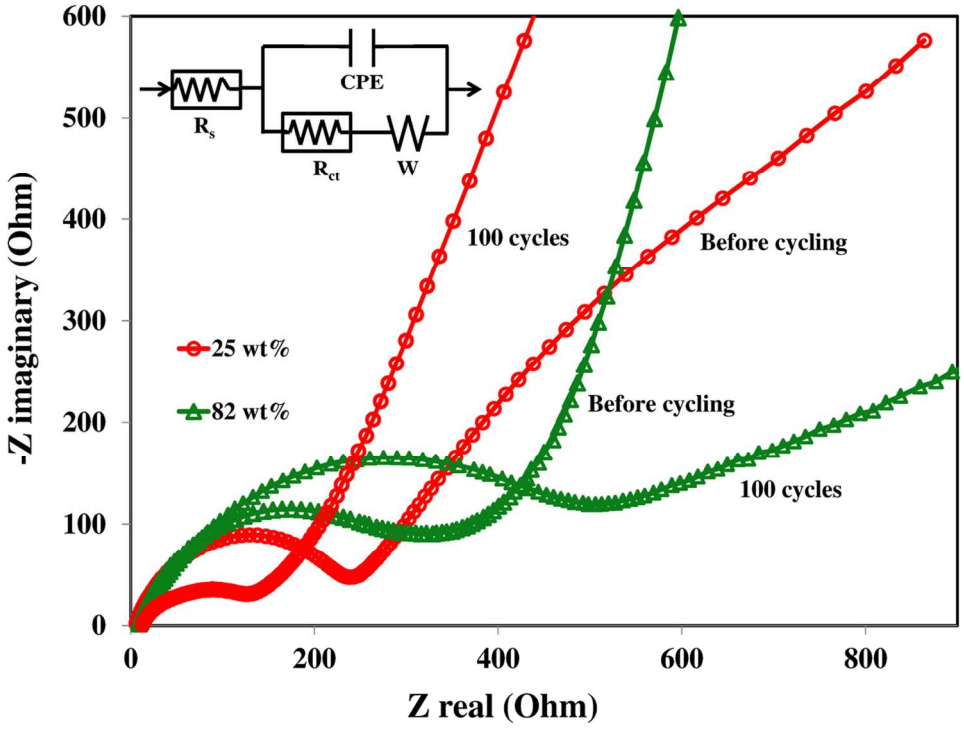

Figure 9. Nyquist plots of 82 and 25 wt% SnO2/graphene anodes before and after 100 discharge/charge cycles.
112x85mm (300 x 300 DPI)

Graphical Abstract

Correlations between microstructure and electrochemical performance of SnO_2/graphene composites with various Sn/C ratios.